

Tectonics

Supporting Information for

Deformation in western Guatemala associated with the NAFCA (North America-Central American Forearc-Caribbean) triple junction: Neotectonic strain localization into the Guatemala City graben

Bridget Garnier¹, Basil Tikoff¹, Omar Flores², Brian Jicha¹, Charles DeMets¹, Beatriz Cosenza-Murales^{1,3}, Walter Hernandez⁴, David Greene⁵

¹University of Wisconsin-Madison, Department of Geoscience, 1215 West Dayton St., Madison, WI 53706

²Centro de Estudios Superiores de Energía y Minas, Edificio T-1, Universidad de San Carlos de Guatemala, Ciudad Universitaria, Zona 12, Guatemala, Guatemala 01012

³Instituto de Investigación en Ciencias Físicas y Matemáticas, Escuela de Ciencias Físicas y Matemáticas, Universidad de San Carlos de Guatemala, Ciudad Universitaria, Zona 12 Guatemala, Guatemala 01012

⁴Retired from the Ministerio de Medio Ambiente y Recursos Naturales, Km. 5 1/2 carretera a Santa Tecla, colonia y calle Las Mercedes, San Salvador, El Salvador

⁵Department of Earth and Environmental Sciences, Denison University, 100 W. College St, Granville OH 43023

Contents of this file

Supplemental Figure A.1 Comparison of GPS site velocities.

Supplemental Figure A.2 Comparison of elastic block models.

Supplemental Figure A.3 Comparison of fault locking solutions and Cocos plate convergence velocities.

Supplemental Text C.1 Additional details from the Santa Domingo Xenacoj outcrop.

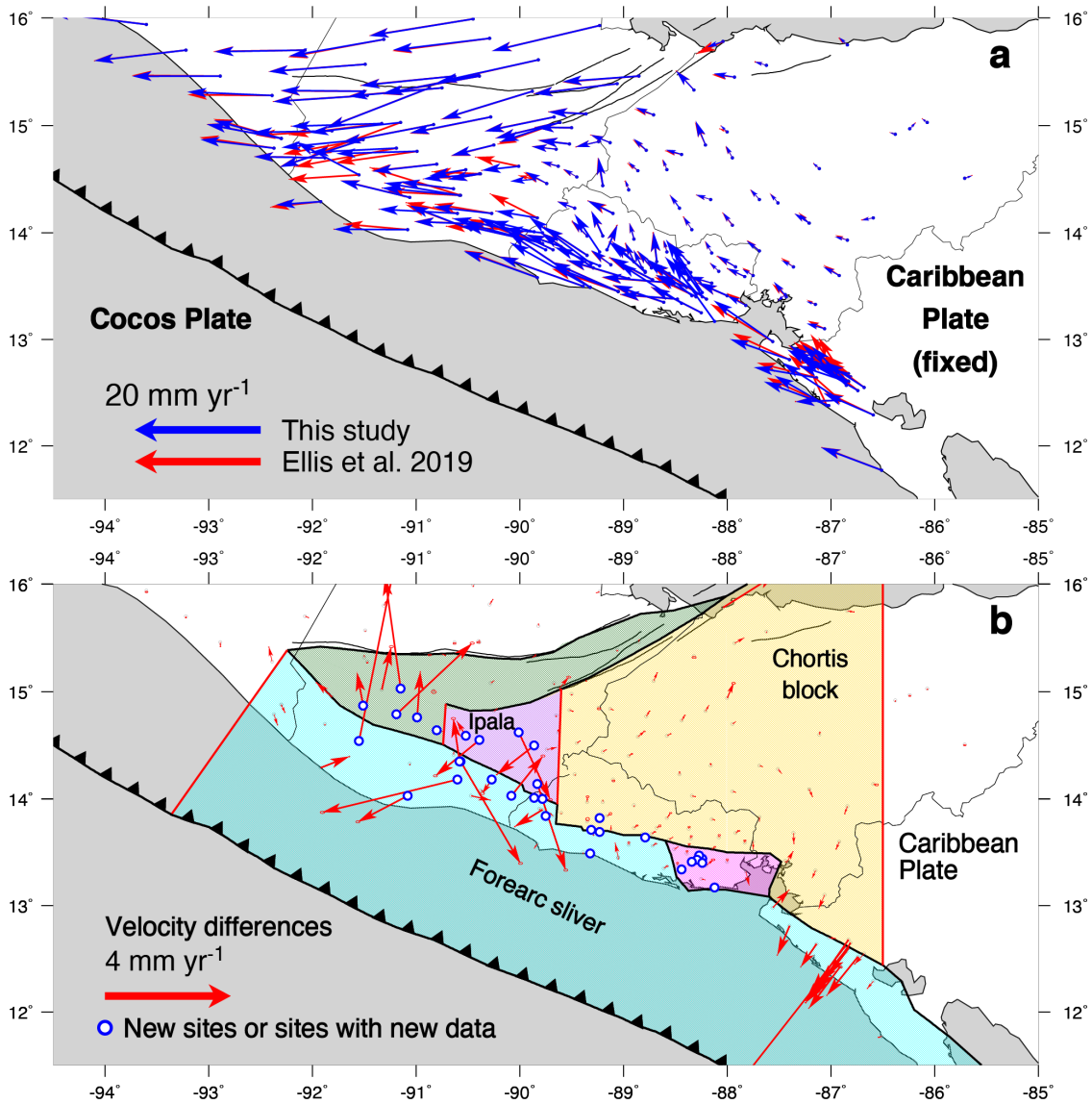
Supplemental Figure C.1 Annotated outcrop photos of the Santa Domingo Xenacoj outcrop transects.

Additional Supporting Information (Files uploaded separately)

Supplemental Table A.1 GPS site velocities and site information.
Supplemental Table A.2 Elastic block model angular velocities.
Supplemental Table B.1 Complete $^{40}\text{Ar}/^{39}\text{Ar}$ data table for west Guatemala samples.

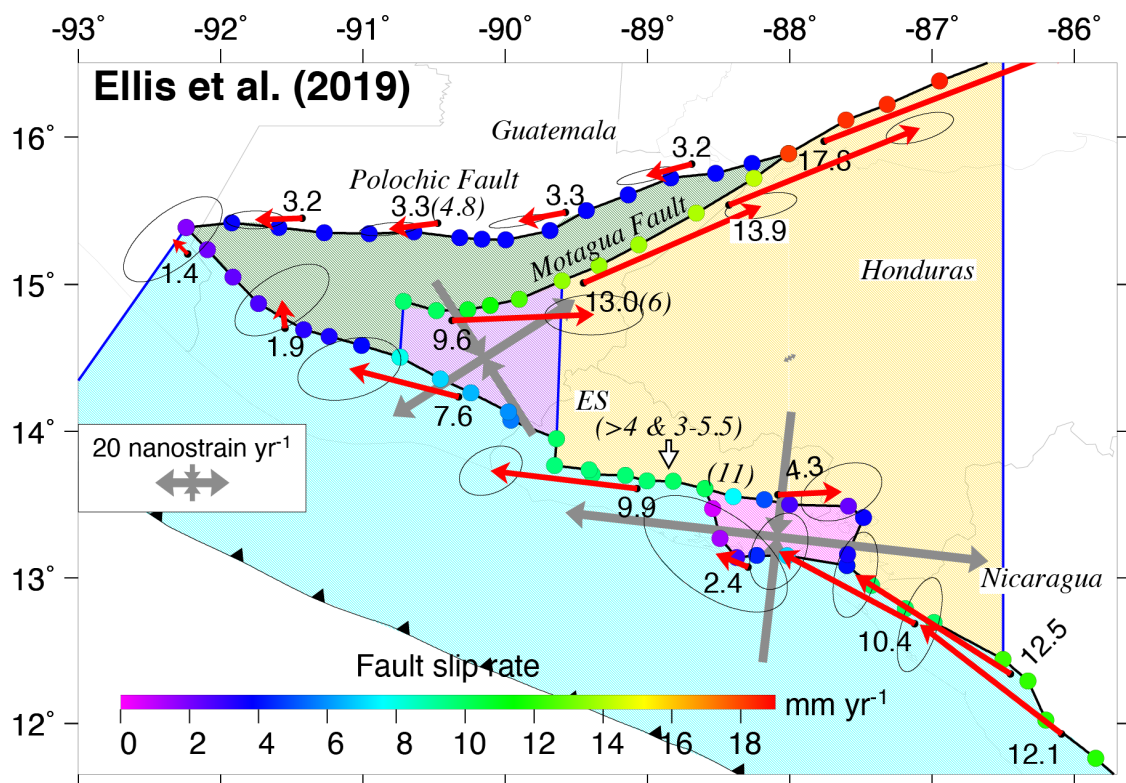
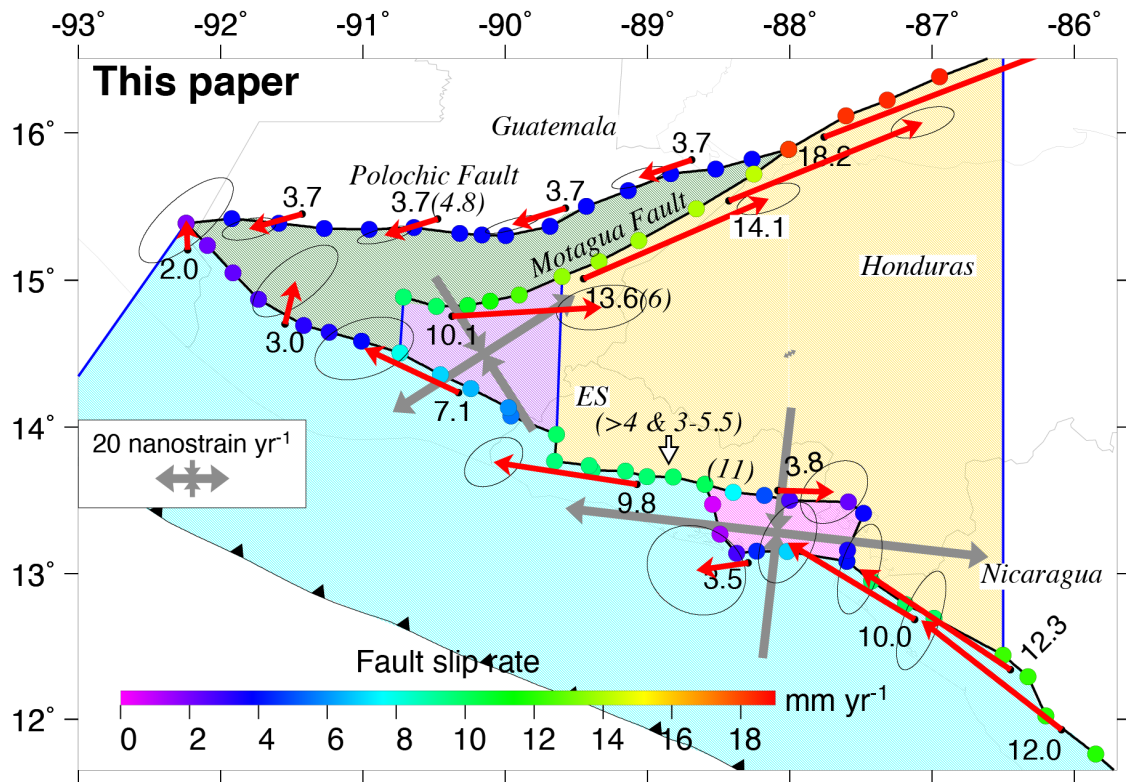
Introduction

The information in the supplemental file contains supporting figures related to the GPS data (Supplemental Figures A.1, A.2, and A.3). The data processing of the GPS data is outlined in the main text

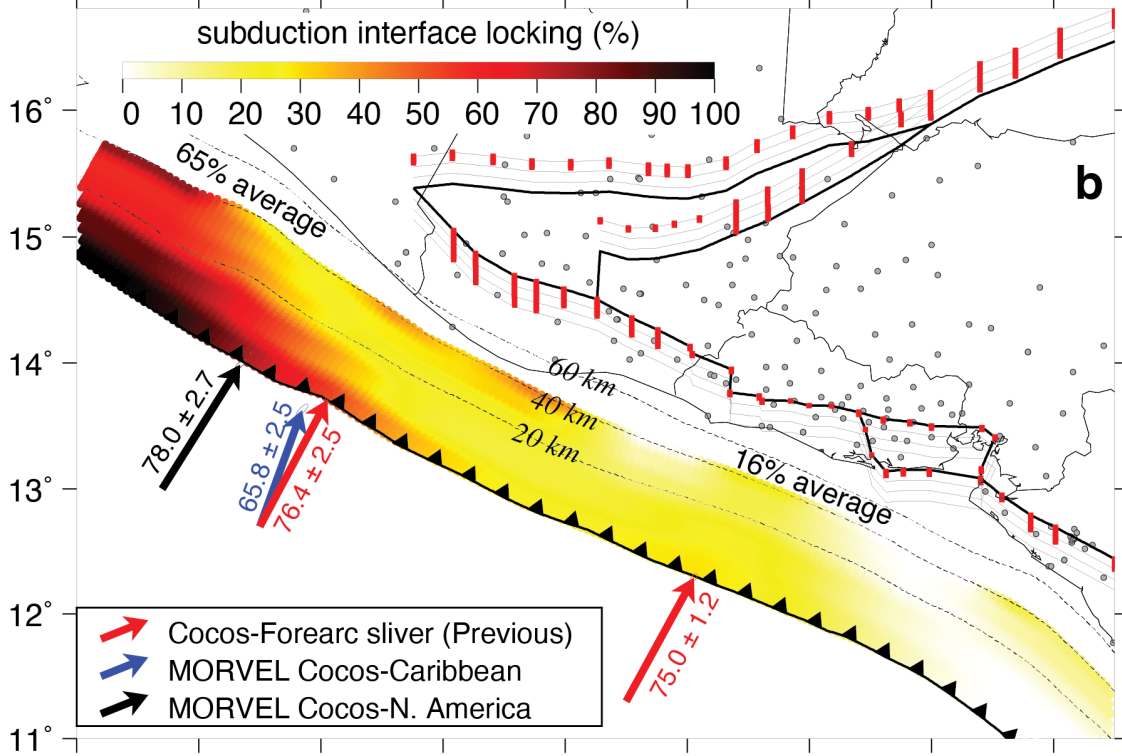
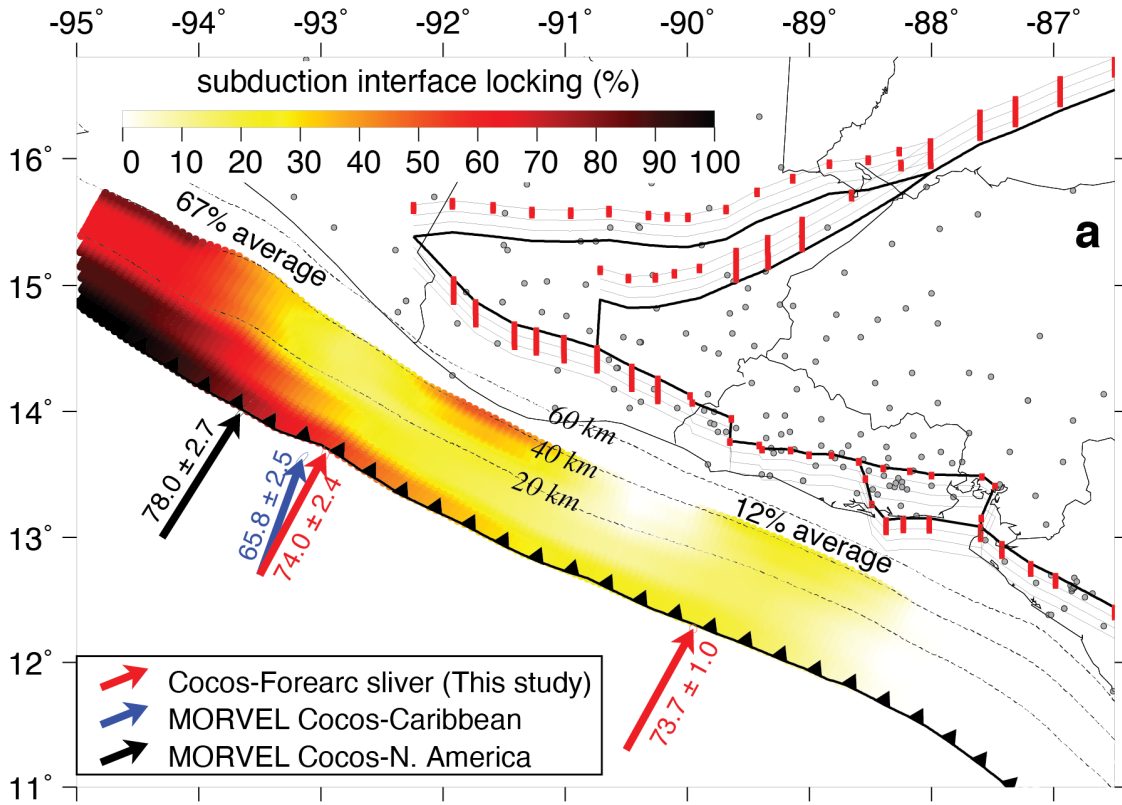


Supplemental Figure A.1. a. Comparison of GPS site velocities in a Caribbean Plate frame of reference for this study and from Ellis et al. (2018; 2019) after corrections for

coseismic offsets and transient afterslip from the 2009 Swan Islands earthquake and the 2012 El Salvador and southern Guatemala earthquakes. The velocity error ellipses are omitted for clarity. b. Blue circles show the locations of GPS sites with new GPS data relative to the data used by Ellis et al. (2019). Red arrows show the GPS site velocities from Ellis et al. (2019) subtracted from the velocities from this study. The shaded regions identify the five blocks for which angular velocities are estimated in our block model inversion.



Supplemental Figure A.2. Predictions of the updated elastic block model estimated in this paper (upper panel) versus those of the Ellis et al. (2019) block model (lower panel). All fault slip rates have units of mm/yr. The slip rates at the strike-slip fault nodes are color coded according to the color scale on the map. Each red arrow and its adjacent number specify the velocity that is estimated for the plate or block on which the arrow originates with respect to the plate or block located on the other side of the adjacent block-bounding fault. The five elastic blocks for which rotation and deformation parameters were estimated in our inversion, which are shaded in the figure, are the same as the blocks identified by Ellis et al. (2019).



Supplemental Figure A.3. Comparisons of new (panel a) and Ellis et al. (2019) (panel b) fault locking solutions and Cocos plate convergence velocities with 1-sigma uncertainties (black, blue, and red arrows). Fault locking is expressed as a percentage of the full fault slip rate. The fence diagrams show perspective depth views of the strike-slip faults downward in 5-km depth intervals. Red circles show the fully locked fault segments and extend downward to the maximum estimated fault locking depth. The shallowest level of each strike-slip fault faces the upper edge of the diagram. The average fault locking values for the moderately and weakly coupled trench segments (northwest and southeast segments, respectively) are nearly the same (67 versus 65 percent and 12 versus 16 percent) for the new and previous models. The black circles in both panels show GPS site locations. All slip rates have units of mm/yr.

Supplemental Text C.1. Additional information from the Santa Domingo Xenacoj outcrop (Xenacoj, Location 1), including the deformational/depositional history.

The Xenacoj outcrop contains more information than we were able to describe in the article. While there is a geologic map of this area by Ritchie (1975) and brief unit descriptions provided by Williams (1960), Koch (1970), and McLean (1970), none of these studies have addressed the large volcanic deposits and faulting that are exposed at the Xenacoj outcrop. Therefore, below, we more thoroughly describe the observed deposits. The units labeled in Figure 4a in the main text and the annotated outcrop photos in Supplemental Figure C.1 (below) represent packages of deposits that are separated by erosional unconformities. The stratigraphic descriptions of the individual deposits of each unit are described below, from oldest to youngest.

Biotite-rich crystal vitric tuff (Biotite tuff, sample 17JF56S). This deposit is exposed as the basement throughout the area, with a maximum observed thickness of 60 meters. The deposit contains angular boulders to cobbles of coarse-grained andesite porphyry, containing biotite, hornblende, and feldspar phenocrysts in a grey aphanitic matrix. The matrix of the deposit as a whole consists of grey ash containing the same phenocrysts observed in the porphyry blocks. Based on the size of the deposit and porphyry blocks, this was a massive deposit with a nearby source. However, no Neogene sources have been identified in this area. This deposit matches a biotite-rich tuff mentioned by Williams (1960) and Ritchie (1975) that underlies much of the area west of the Guatemala City graben and north of the Pan-American highway, but these works did not thoroughly map or investigate the unit.

$^{40}\text{Ar}/^{39}\text{Ar}$ age dating of this deposit produced an age of 9.117 ± 0.006 Ma, which puts it within the span of Miocene volcanic deposits observed behind the current volcanic arc across Guatemala. XRF and ash mineralogy are documented in the article.

Unit 1. (*a, Sample 17JF56A*) The oldest deposit in Unit 1 is a tan vitric tuff containing phenocrysts, glass fragments, ash, lithics, and no pumice fragments. The deposit has a sandy texture from the fine-grained matrix. $^{40}\text{Ar}/^{39}\text{Ar}$ age dating produced an age of 1.495 ± 0.057 Ma, which is older than the Quaternary tephra stratigraphy by Koch and

McLean (1975) and Rose et al. (1999). XRF and ash mineralogy are documented in the article. This unit is slightly folded and contains numerous normal faults.

(b) The overlying deposit is a lithic mudstone containing felsic and mafic lithics and phenocrysts in a silt/mud matrix. Paleosol overlies the deposit.

-----EROSIONAL UNCONFORMITY – Cuts across the paleosol of Unit 1.

Unit 2. Only a small portion of this deposit is exposed on the outcrop. However, we did not do a description of this deposit.

-----EROSIONAL UNCONFORMITY

Unit 3. Unit 3 contains at least 3-4 tephtras of varying color and thickness.

(c) This sequence contains two light colored deposits with overlying paleosols. It gives it a unique striped appearance.

(d) Clast-supported conglomerate containing felsic and mafic (10%) angular clasts and millimeter-sized grains of plagioclase and quartz in a red/tan matrix.

(e) Unit has a basal white ash tuff containing few millimeter-sized pumice fragments and plagioclase and mafic phenocrysts. An upper grey portion has two thin, white ash deposits near the boundary between the white and grey deposits.

(f, *Sample 17JF56R*) Massive tephtra that contains white pumice, some with orange or pink staining, that have linear vesicles and phenocrysts of plagioclase, amphibole, and biotite. The ash matrix contains phenocrysts found in the pumice. XRF and pumice mineralogy are described in the article. $^{40}\text{Ar}/^{39}\text{Ar}$ dating produced an age of 1.145 ± 0.061 Ma, which is older than the Quaternary tephtras described in the literature.

-----EROSIONAL UNCONFORMITY

Unit 4. Unit 4 is more than 40 m thick and contains unfaulted tephtras, reworked deposits, and paleosols. This unfaulted section was thoroughly documented by co-author Walter Hernandez in January 2019. His descriptions are summarized as follows:

(g) Two deposits make up this package, each with an overlying paleosol. The lower deposit is a beige-colored, lightly weathered, and indurated pyroclastic flow of felsic composition. The upper deposit is a pale-brown, highly weathered pyroclastic surge of andesitic composition.

(h) This package contains three pyroclastic deposits and is ~10m thick. The basal deposit is a pumice fall, moderately sorted, white to beige in color, and weathered. The middle deposit consists of an 8-meter sequence of pyroclastic surges that are banded and stratified, weathered to a reddish-brown color, and seem to be of andesitic composition. The upper deposit consists of a white, stratified, pyroclastic surge deposit that is lightly weathered and possibly dacitic in composition. No paleosols are visible between the three deposits.

(i) The base contains a thin layer of pumice fall, light in color, somewhat sorted, and weathered with an overlying paleosol. The pumice layer and paleosol together are one meter thick and the pumice layer thins towards the main fault.

(j) This package is ~10 meters thick and contains 8 thin volcanic deposits that are fine-grained, banded, compact, light brown, and appear dacitic in composition. Each deposit is separated by a paleosol. Layers are parallel to each other. Slight erosion took place before the deposition of the overlying deposit.

(k) This deposit consists of a 50-70 cm thick fine ash, with an overlying 75 cm thick, brown paleosol. The ash deposit appears light gray on the weathered surface, but is light brown to beige on a fresh surface. Erosion took place before deposition of overlying deposit.

(l) The base on this sequence is a thin (25-45 cm), light brown, indurated, fine ash deposit, with a 1.9-2.25 m overlying paleosol. Deposit may be andesitic or basaltic in composition.

(m) This package consists of three brown, weathered ash deposits. The lower ash deposit, possibly andesitic composition, is 70 cm thick with a 1.3 m paleosol. The middle deposit is similar in appearance, with a thickness of 1.7 m and an overlying 85 cm paleosol. The upper ash layer is a third paleosol. Slight erosion appears to have occurred between each layer.

(n, *Samples 17JF56J and WH19S6*) This deposit contains several layers of pumice, the basal layer is white with the remaining being yellow to brown. Pumice layers have differing thickness and grain sizes, but come to a total thickness of 4.36 m. The pumice layers also contain euhedral golden and black biotite crystals, as well as crystals of plagioclase, hornblende, and magnetite. Pumice layers show reverse grading with a thin layer of ash atop each one. The similarity in the appearance and composition of the pumice and ash layers suggests that the sequence come from that same source and eruptive event, that had an oscillatory nature and very energetic at the end with a final eruption of pumice. A 27 cm paleosol overlies the pumice layers and contains varied lithics. Two samples were taken from this layer. The pumice mineralogy analysis from sample 17JF56J and the XRF data from sample WH19S6 are in the article. This layer was correlated to the E tephra of the Amatitlan caldera.

(o) White to beige, fine ash deposit (1.7 m thick) with an overlying paleosol (65 cm thick).

(p) Thin fine ash deposit (20 cm thick) with an overlying paleosol (70 cm thick).

(q, *Sample WH19S5*) This sequence is the highest of the unit, with three thin felsic tephra separated by paleosols. Tephra have similar thicknesses of (from lower to upper) 1.15 m, 1.17 m, and 1.3 m. The basal tephra contains white pumice with a light brown ash matrix, well indurated. The middle tephra contains a basal pumice layer with reverse grading and moderately sorted, white in color, and poorly indurated. The upper layer contains pumice, is slightly yellow, and poorly indurated. Yellow pumice has fine and light vesicles and contains phenocrysts of plagioclase, hornblende, and few opaque mafics. XRF analysis was applied to a sample of this unit and is displayed in the article.

-----EROSIONAL UNCONFORMITY

Unit 5. Layered paleochannel that cut through the volcanic deposits and deposited volcanic and reworked material.

Unit 6. This deposit consists of reworked volcanic material that was deposited in the channel in a high energy matter, that filled the channel with poorly sorted, angular blocks material. There appears to be a main channel and two secondary channels.

-----EROSIONAL UNCONFORMITY

Unit 7. A final sequence of 2-3 deposits overlying all the previous deposits. These layers were unable to be sampled or observed directly, but the form indicates that they were

deposited after an erosional event, blanketing any irregularities in the surface and are currently flat lying. A final paleosol is the current soil layer.



Supplemental Figure C.1. Annotated outcrop photos of transects A and B from the Xenacoj outcrop. Units and individual deposits are labeled with letters used in the text.